Journal Pre-proof

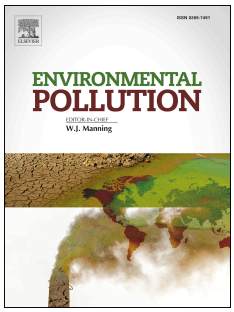

Interrogating cadmium and lead biosorption mechanisms by *Simplicillium chinense* via infrared spectroscopy

Zhongmin Jin, Lin Xie, Tuo Zhang, Lijie Liu, Tom Black, Kevin C. Jones, Hao Zhang, Xinzi Wang, Naifu Jin, Dayi Zhang

PII: S0269-7491(20)30853-8

DOI: https://doi.org/10.1016/j.envpol.2020.114419

Reference: ENPO 114419

To appear in: *Environmental Pollution*

Received Date: 5 February 2020

Revised Date: 29 February 2020

Accepted Date: 18 March 2020

Please cite this article as: Jin, Z., Xie, L., Zhang, T., Liu, L., Black, T., Jones, K.C., Zhang, H., Wang, X., Jin, N., Zhang, D., Interrogating cadmium and lead biosorption mechanisms by *Simplicillium chinense* via infrared spectroscopy, *Environmental Pollution* (2020), doi: https://doi.org/10.1016/j.envpol.2020.114419.

CRediT author statement

Zhongmin Jin: Investigation, Supervision, Writing- Original draft preparation. Lin Xie: Data curation, Visualization. Tuo Zhang: Investigation, Data curation. Lijie Liu: Data curation. Tom Black: Investigation, Data curation. Kevin C Jones: Resources, Data curation. Hao Zhang: Resources, Data curation. Xinzi Wang: Data curation, Visualization. Naifu Jin: Investigation, Data curation, Visualization, Writing- Original draft preparation. Dayi Zhang: Conceptualization, Methodology, Resources, Writing- Original draft preparation, Writing- Reviewing and Editing.

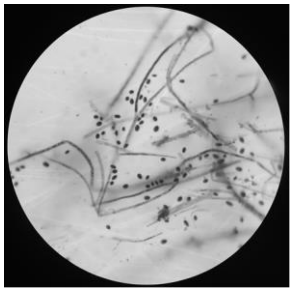

Simplicillium chinense

Cultivation with 48 carbons sources on PM4 plate

Pb biosorption

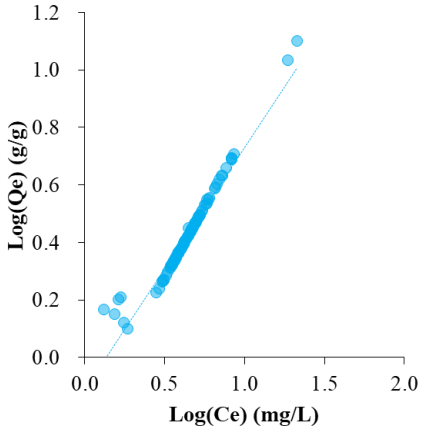

Freundlich isotherm

No biomarker for Pb biosorption

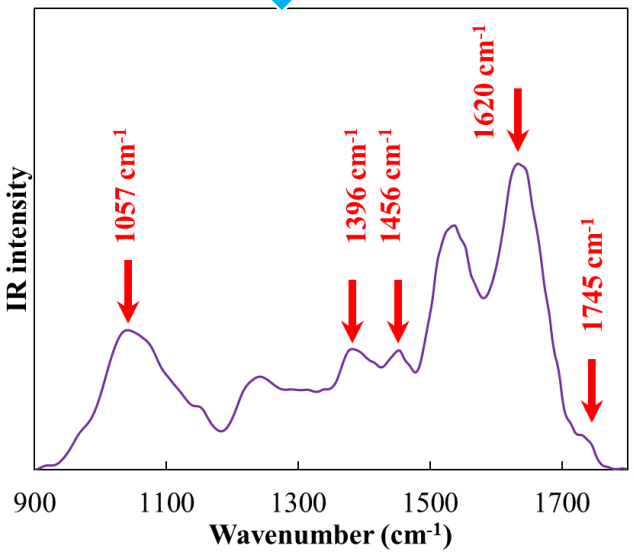

Five biomarkers for Pb biosorption

Langmuir isotherm

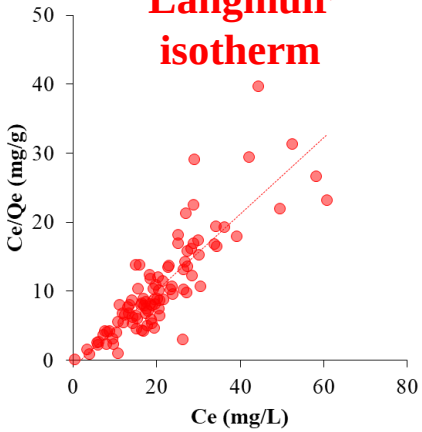

Cd biosorption

Interrogating cadmium and lead biosorption mechanisms by *Simplicillium chinense* via infrared spectroscopy

Zhongmin Jin[1,2], Lin Xie[1], Tuo Zhang[3], Lijie Liu[1], Tom Black[2], Kevin C Jones[2], Hao Zhang[2], Xinzi Wang[2], Naifu Jin[4], Dayi Zhang[4,*]

1. College of Agriculture, Forestry and Life Science, Qiqihar University, Qiqihar 161006, PR China
2. Lancaster Environment Centre, Lancaster University, Lancaster LA1 4YQ, UK
3. College of Environmental Science and Engineering, China West Normal University, Nanchong 637002, PR China
4. School of Environment, Tsinghua University, Beijing 100084, PR China

***Corresponding author**

Dr Dayi Zhang

School of Environment, Tsinghua University, Beijing, 100084, PR China

Tel.: +86(0)1062773232; Fax: +86(0)1062785687

Email: zhangdayi@tsinghua.edu.cn

Abstract

Fungi-associated phytoremediation is an environmentally friendly and cost-efficient approach to removal potential toxic elements (PTEs) from contaminated soils. Many fungal strains have been reported to possess PTE-biosorption behaviour which benefits phytoremediation performance. Nevertheless, most studies are limited in rich or defined medium, far away from the real-world scenarios where nutrients are deficient. Understanding fungal PTE-biosorption performance and influential factors in soil environment can expand their application potential and is urgently needed. This study applied attenuated total reflection Fourier-transform infrared (ATR-FTIR) coupled with phenotypic microarrays to study the biospectral alterations of a fungal strain *Simplicillium chinense* QD10 and explore the mechanisms of Cd and Pb biosorption. Both Cd and Pb were efficiently adsorbed by *S. chinense* QD10 cultivated with 48 different carbon sources and the biosorption efficiency achieved >90%. As the first study using spectroscopic tools to analyse PTE-biosorption by fungal cells in a high-throughput manner, our results indicated that spectral biomarkers associated with phosphor-lipids and proteins (1745 cm^{-1}, 1456 cm^{-1} and 1396 cm^{-1}) were significantly correlated with Cd biosorption, suggesting the cell wall components of *S. chinense* QD10 as the primary interactive targets. In contrast, there was no any spectral biomarker associated with Pb biosorption. Addtionally, adsorption isotherms evidenced a Langmuir model for Cd biosorption but a Freundlich model for Pb biosorption. Accordingly, Pb and Cd biosorption by *S. chinense* QD10 followed discriminating mechanisms, specific adsorption on cell membrane for Cd and unspecific extracellular precipitation for Pb. This work lends new insights into the mechanisms of PTE-biosorption *via* IR spectrochemical tools, which provide more comprehensive clues for biosorption

behaviour with a nondestructive and high-throughput manner solving the traditional technical barrier regarding the real-world scenarios.

Keywords: cadmium, lead, biosorption, phytoremediation, carbon sources, ATR-FTIR spectrosocpy

1. Introduction

With the increasing development of many metal-related industries, *e.g.*, metal mining, matal surface treating, energy production and fertilizer manufacturing, some metals (mercury, chromium, etc.) or non-metals (arsenic, selenium, etc.) possessing potential toxicities to human health are named as potential toxic elements (PTEs) and have become one of the most critical sources of environmental contamination (Dong et al., 2010). Industrial residues containing PTEs are continuously discharged into the environment, posing vital threats to human life and ecosystems (Dong et al., 2010; Liu et al., 2013). PTE-induced toxicity has been recognized to last for an extended time in nature and accumulate in the food chain. The presence of PTEs even in traces is harmful to both flora and fauna, cadmium (Cd) exposure for instance, which may cause irreversible tubular damage in kidney (Järup, 2003; Leonard et al., 2004). Numerous PTE-contaminated sites have been identified and require remediation (Huang et al., 2019; Jiang et al., 2019).

To remediate PTE-contaminated soils and reduce the exposure possibility, several approaches are developed and applied, including solidification (Tantawy et al., 2012), elution (Rui et al., 2019), phytoremediation (Jiang et al., 2018; Jin et al., 2019). Stabilization aims to adsorb or reduce PTEs, transferring unstable PTEs into stable phases with less availability, *e.g.*, hydroxides and minerals (Wang and Vipulanandan, 2001; Yuan et al., 2018). Stabilizers include natural minerals (Gheju et al., 2016), modified minerals (Ou et al., 2018; Sha et al., 2018; Singh et al., 2017), synthetic materials (Liu et al., 2014; Sarkar et al., 2010), and reductive reagents (Geelhoed et al., 2003; Patterson et al., 1997). However, the long-term stability of stabilization strategy remains doubtful. Elution uses solvents to form PTE-chelates and enhance PTE mobility (Khan et al., 2010), but suffers from the poor efficiency in clay-rich soils

owing to the relatively smaller osmotic coefficient which significantly abates PTE mobility (Bolan et al., 2014; Rui et al., 2019). Biosorption which uses biomaterials (bacteria, fungi, yeasts and plants) is highlighted as an alternative remediation approach for PTEs (Wang and Chen, 2006). Comparing to other approaches, biosorption is relatively cost-efficient, particularly for soils with low PTE levels (Yan and Viraraghavan, 2003) or co-contaminated with other organic compounds (Deng et al., 2018b). Phytoremediation is environmentally friendly to clean PTE-contaminated soils and remain soil functions (Wiszniewska et al., 2016). Plants generally handle the contaminants without damaging soil properties via an enormous ability to uptake and detoxify PTEs by various mechanisms, such as uptake by roots, translocation to aerial tissues and PTE- complexion with organic substances (Ali et al., 2013; Liu et al., 2019).

In the soil ecosystem, the major soil biomass and biodiversity are formed by microorganisms (Jin et al., 2019). Their presence in the rhizosphere plays important roles in PTE phytoremediation (Jin et al., 2019; Khan, 2005). Cr phytoremediation, for instance, is only effective for exchangeable or available Cr in soils (Shaheen et al., 2019). Most phytoremediation practices use soil microbes or leaching reagents to enhance PTE removal performance since their availability is strongly linked with soil microbial activities (Deng et al., 2018a; Yin et al., 2015). Fungi, as one critical group of microorganisms, have been applied as metal biosorbents in phytoremediation in prior studies (Say et al., 2001). PTE biosorption capability of *Saccharomyces Cerevisiae* ranges from 10 to 300 mg/g dry-cell-weight (DCW) for lead (Pb) and 10 to 100 mg/g DCW for Cd (Wang and Chen, 2006). *Penicillium* sp. MRF-1 has a strong Cd biosorption capacity (0.13-9.39 mg/g DCW) (Velmurugan et al., 2010) and the maximum biosorption capacity of *Exiguobacterium sp.* is 15.6 mg/g DCW for Cd

(Park and Chon, 2016). The mechanisms of fungal PTE biosorption are complicated and mainly consist of two key stages: direct adsorption on fungal membrane and penetration through cell wall. The first stage is a passive biosorption process independant on fungal metabolism, and the key influential factor is the functional groups on cell membrane which affect the interactions between fungal cells and PTE ions (Leonard et al., 2004). In the second stage, PTE ions penetrate the cell membrane and enter cells *via* active biosorption, and it is dependent on fungal metabolism and related to the transportation and deposition of PTEs (Leonard et al., 2004). Accordingly, from the eventual allocation of PTEs within cells, biosorption can be classified as extracellular accumulation or precipitation, cell surface sorption or precipitation, and intracellular accumulation (Veglio and Beolchini, 1997). However, most previous studies address fungal PTE biosorption in rich or defined media with limited carbon sources, not able to represent their phenotypic features and biosorption performance in real-world scenarios, where the biosorption process is influenced by many environmental variables, such as PTE availability, carbon sources and growth conditions (Hamdy, 2000; He and Chen, 2014; Wang and Chen, 2014). It is of great importance to inspect microbial phenotypic features and PTE biosorption capabilities across a wide range of environmental conditions representing real-world scenarios, and a reliable and high-throughput analytical method is urgently required.

Biospectroscopy as a group of interdisciplinary tools has many advantages in microbiological study owing to their measurement attributes with a high-throughput, nonintrusive and nondestructive manner (Heys et al., 2014; Jin et al., 2020; Jin et al., 2017a; Li et al., 2017; Martin et al., 2010). Infrared (IR) spectroscopy, for instance, relies on the principle that the energy from the infrared radiation is absorbed by the bending, stretching and twisting of bonds (C-H, O-H, N-H, C=O, C-C, etc.) within the

sample, resulting in characteristic transmittance and reflectance patterns (Martin et al., 2010; Naumann et al., 2005). Previous spectroscopic studies have successfully detected the presence of fungal cells, characterized fungal species, and diagnosed fungi-induced diseases (Gordon et al., 1999; Kos et al., 2002; Naumann et al., 2005). Recently, biospectroscopic approaches are expanded to determine microbial interactions with environmental stimuli, *e.g.*, antibiotic resistance (Jin et al., 2017a; Jin et al., 2017b), showing great potentials in studying PTE-biosorption processes and bringing new insights into the relevant mechanisms. Yet, no such attempt is reported.

The present study applied attenuated total reflection Fourier-transform infrared (ATR-FTIR) spectroscopy coupled with phenotype microarrays to characterize the biosorption of Cd and Pb by a fungal strain *Simplicillium chinense* QD10 cultivated with 48 different carbon sources. This is the first study using spectrochemical tool to analyse fungal PTE-biosorption process and investigate the impacts of carbon sources in a high-throughput and nondestructive manner. Our results aimed to provide a valuable spectroscopic database to look deeper into the biosorption mechanism from a novel perspective and offer new clues to enhance fungi-associated phytoremediation by altering the metabolic activities and biosorption performance of fungal cells in real-world scenarios.

2. Materials and Methods

2.1 Strains and cultivation condition

The fungal strain *Simplicillium chinense* used in this study was isolated in soils from Zhalong Wetland (47°32'30"N, 124°37'50"E, Qiqihar City, China) in October 2015. It was named as *S. chinense* QD10 and had a satisfactory biosorption performance for Cd and Pb (Jin et al., 2019). This strain was cultivated in potato dextrose medium

(200 g of potato, 20 g of glucose and 20 g of agarose dissolved in 1,000 mL of deionized water and autoclaved) at 28°C for 5 days. Subsequently, the cells were washed and resuspended in deionized water as stock solution for further treatment. Cd and Pb stock solutions were prepared by dissolving $Pb(NO_3)_2$ and $CdSO_4$ in deionized water, respectively. The final concentration of Cd and Pb in stock solution was 1.0 g/L.

PM1 plate (BIOLOG, Hayward, CA, USA) was used to examine the carbon metabolic features of *S. chinense* QD10. Fifteen microliters of the cell stock solution were resuspended in 135 µL of minimal medium (Zhang et al., 2011) and then added into each well of a PM1 plate. Each well was then supplemented with 1.5 µL of Redox Dye Mix A (100×, BIOLOG, Hayward, CA, USA) to monitor fungal growth. The plate was incubated at 30ºC for 5 days, and the colour development was measured every 4 hours for the absorbance at 590 nm wavelength (respiratory unit, RU) by a multimode microplate reader (FLUOstar Omega, BMG Labtech, UK). To avoid the influence of Redox Dye on fungal biospectra, another treatment was prepared following the same protocol except for the addition of Redox Dye Mix A, and used for biospectral analysis. All the treatments were carried out in triplicates.

2.2 Cd/Pb biosorption treatment and chemical analysis

After 5-day cultivation, each well of PM1 plate was subjected with 20 µL of Pb or Cd stock solution and kept shaking for 2 hours (final Pb or Cd concentration of 100 mg/L). Subsequently, the supernatant was collected after 3,000-rpm centrifugation for 20 min. The cell pellets were further washed with 5 mL deionized water and centrifuged again (3,000 rpm) for another 20 min. The supernatants from two-step centrifugation were combined, spiked with 20 µL of internal standards (^{103}Rh, ^{45}Sc,

^{209}Bi), and diluted with deionized water to a final volume of 50 mL for metal analysis. Cd and Pb were analyzed by inductively coupled plasma mass spectrometry (ICP-MS, X-series 2, Thermo Scientific, USA), and the detection wavelength was 228.8 and 283.3 nm, respectively. The standard calibration solution contained a mixture of Cd and Pb in HNO_3 (0.1 M), ranging from 0 to 100 μg/L.

2.3 Infrared spectra measurement

Cell pellets after biosorption were further washed three times with sterile deionized water to remove the residues of growth media and resuspended in 70% ethanol for fixation. The washed cell pellets (minimal amount >5 μL) were applied onto Low-E slides for interrogation by ATR-FTIR spectroscopy. A TENSOR 27 FTIR spectrometer (Bruker Optics Ltd., UK) equipped with a Helios ATR attachment (containing a diamond internal IRE; incidence angle of the IR beam: 45°) was used and the instrument parameters were set as 32 scans and spatial resolution of 8 cm^{-1}. Before the measurement of a new sample, the crystal was cleaned with deionized water, and the background readings were retaken. A total of 20 spectra were acquired for each treatment.

2.4 Data analysis

The RU of fungal cells was analysed by MARS software (BMG Labtech, UK). The relative RU for fungal growth with each carbon source was calculated as the mean of all RUs measured on day 5. The growth index (GI) of fungal cells cultivated with different carbon source was calculated in Equation (1).

$$\mathrm{GI}_n = \frac{[\text{Relative RU}]_n}{[\text{Relative RU}]_{A1}} - 1.0 \quad (2)$$

Here, GI_n refers to the GI in *n*th well. $[\text{Relative RU}]_n$ and $[\text{Relative RU}]_{A1}$

194 represent the relative RU in *n*th well and well A1 (no carbon source, negative control),
195 respectively.

196 Fungal biomass was obtained by drying the cell pellets and measuring the weight with
197 the unit of dry cell weight (DCW). The linear regression between the GI and biomass
198 was obtained by serially diluted fungal suspension with the known GI and biomass,
199 following Equation (2).

200 $$\text{Biomass} = 0.196 \times \text{GI} + 0.168 \quad (2)$$

201 The initial spectral data generated from ATR-FTIR spectroscopy were analyzed
202 within MATLAB R2011a software (TheMathsWorks, Natick, MA, USA), coupled
203 with IrootLab toolbox (http://irootlab.googlecode.com) (Trevisan et al., 2013). Unless
204 otherwise stated, the acquired spectra were truncated to the biochemical-cell
205 fingerprint region (1800-900 cm^{-1}), rubberband baseline corrected and normalized to
206 Amide I (1650 cm^{-1}) (Baker et al., 2014; Martin et al., 2010). Second order
207 differentiation baseline correction and vector normalization were also performed as an
208 alternative mean to process the data. Cross-calculation principal component analysis
209 followed by linear discriminant analysis (PCA-LDA) was subsequently applied to the
210 preprocessed data to reduce the number of spectra to 10 uncorrelated principal
211 components (PCs), which account for >99% of the total variance; LDA is a
212 supervised technique coupled with PCA in order to maximize inter-class and
213 minimize intra-class variance (Martin et al., 2010). To identify the specific IR bands
214 associated with fungal growth and biosorption efficiency of Pb or Cd, cluster vector
215 approach was conducted and visualized the discriminating difference (Butler et al.,
216 2015; Martin et al., 2010). The relationships between each IR band intensity and GI,
217 Pb biosorption efficiency or Cd biosorption efficiency across media supplemented

with 48 carbon sources were analysed by Pearson correlation analysis ($p<0.05$). All the statistical analyses were carried out in GraphPad Prism 6 unless specific statement.

3. Results

3.1 S. chinense QD10 growth profiles cultivated with 48 carbon sources

The growth curves of *S. chinense* QD10 obtained from the RU measurement illustrated significant differences across media supplemented with 48 carbon sources (Figure 1A). In all treatments, an obvious lag phase lasted for about 8 hours, followed by a dramatical increasing RU for some carbon sources. After the logarithmic growth phase, *S. chinense* QD10 entered the stationary phase at 72 hours. These results demonstrated that *S. chinense* QD10 could effectively utilize some carbon sources and achieve satisfactory growth for 3 days. Figure 1B illustrated that the four carbon sources possessing significantly higher GI (>1.0) were L-glutamine, Tween 80, glycolic acid and methylpyruvate. Fourteen carbon sources moderately supporting the growth of *S. chinense* QD10 (0.5<GI<1.0) included α-hydroxyglutaric acid-g-lactone, α-hydroxybutyric acid, adenosine, Gly-Asp, fumaric acid, bromosuccinic acid, glyoxylic acid, D-cellobiose, inosine, Gly-Glu, tricarballylic acid, p-hydroxyphenyl acetic acid, m-hydroxyphenyl acetic acid, and 2-aminoethanol. Other carbons sources were barely useable by *S. chinense* QD10 as the GI was <0.5. Based on the molecular structure and functional groups, 48 carbon sources were categorized into five groups as nucleic acids, carbohydrates, carboxylic acids, amino acids and others. There was no significant difference in fungal growth between the five groups of carbon sources ($p>0.05$).

3.2 Cd and Pb biosorption by S. chinense QD10 cultivated with 48 different carbon sources

Both Cd and Pb were efficiently adsorbed by *S. chinense* QD10 cultivated in minimal medium with 48 different carbon sources, and the biosorption efficiency achieved >90% for all treatments (Table S1 in Electronic Supporting Information, ESI). Two adsorption equilibrium models (Langmuir and Freundlich) were applied to understand Cd and Pb biosorption mechanisms by *S. chinense* QD10. The Langmuir isotherm model represents the monolayer adsorption mechanism with a restriction of no stacking of adsorbed molecules, as described in Equation (3). The Freundlich isotherm model represents both monolayer and multilayer adsorptions by considering the heterogeneous surfaces possessing different sorption energy sites, as described in Equation (4).

$$Q_e = Q_{max} \frac{K_L C_e}{1 + K_L C_e} \quad (3)$$

$$Q_e = K_F C_e^{1/n} \quad (4)$$

Here, Q_e (mg/g DCW) refers to the total Cd/Pb biosorption capacity, and C_e (g/L) represents the equilibrium Cd/Pb concentration in the liquid phase. Q_{max} (mg/g DCW) is the maximum Cd/Pb biosorption capacity for monolayer adsorption in Langmuir isotherm model, and K_L (L/mg) is the Langmuir constant associated with adsorption energy. K_F (mg/g DCW) represents Cd/Pb biosorption capacity in both monolayer and multilayer mechanism in Freundlich isotherm model, and 1/?? is the heterogeneous sorption sites. Either Langmuir or Freundlich isotherm model can be expressed in a linear form as shown in Equations (5) and (6), respectively.

$$\frac{C_e}{Q_e} = \frac{1}{Q_{max} \cdot K_L} + \frac{C_e}{Q_{max}} \quad (5)$$

$$\log Q_e = \log K_F + \frac{1}{n} \times \log C_e \quad (6)$$

Figure 2A illustrates that Cd biosorption fits better with Langmuir isotherm (R^2=0.7324) than Freundlich isotherm (R^2=0.0653). The maximum Langmuir biosorption capacity (Q_{max}) is 1.81 (mg/g DCW) and the Langmuir constant associated with adsorption energy (K_L) is 1.75 L/mg. In contrast, Pb biosorption fits better with Freundlich isotherm (R^2=0.9458) than Langmuir isotherm (R^2=0.1121, Figure 2B). The empirical parameter related to heterogeneous sorption site (1/n) is 0.84 and the biosorption capacity (K_F) is 0.77 (mg/g DCW) in Freundlich isotherm.

3.3 Infrared spectra of S. chinense QD10 cultivated with 48 different carbon sources

In general, *S. chinense* QD10 shared similar infrared spectra across 48 different carbon sources regarding the cellular structures (Figure 3A), including lipid (~ 1750 cm^{-1}), Amide I (~ 1650 cm^{-1}), Amide II (~ 1550 cm^{-1}), Amide III (~ 1260 cm^{-1}), carbohydrate (~ 1155 cm^{-1}) and symmetric phosphate stretching vibrations (~ 1080 cm^{-1}). The 1D score plot of PCA-LDA (Figure 3B) indicated the variations between each category of carbon source, and one-way ANOVA test coupled with Turkey's multiple comparisons demonstrated that the biospectra in the five groups of carbon sources were significantly differentiated (p<0.05), except for the variation between the groups of amino acids and others (p>0.05).

The cluster vector analysis reveals more information regarding the biomolecular difference (Figure 4), which includes five primary peaks derived from original spectra as relevant biomarkers for each group of carbon sources. More precisely, the biomarkers of *S. chinense* QD10 cultivated with amino acids are (~1134 cm^{-1}), PO_2^- asymmetric (~ 1265 cm^{-1}), Amide III (~ 1185 cm^{-1}), Amide II (~ 1517 cm^{-1}) and C=O

(~ 1728 cm^{-1}). Besides the peak of PO_2^- asymmetric (~ 1265 cm^{-1}), other significant peaks of carbohydrate-cultivated *S. chinense* QD10 cells are RNA (~ 1117 cm^{-1}), CH in-plane bend (~ 1510 cm^{-1}), Amide I (~ 1659 cm^{-1}) and C=O, lipids (~ 1740 cm^{-1}). In nucleic acid group, the characteristic peaks are *v*(CO), *v*(CC) (~ 1018 cm^{-1}), deoxyribose (~ 1188 cm^{-1}), (~ 1269 cm^{-1}), Amide II (~ 1540 cm^{-1}) and lipids (~ 1740 cm^{-1}). For carboxylic acid group, the characteristic peaks include stretching vibrations of hydrogen-bonding, C-OH groups (~ 1153 cm^{-1}), N-H thymine (~ 1276 cm^{-1}), C=C, deformation C-H (~ 1496 cm^{-1}), Ring base (~ 1555 cm^{-1}), base carbonyl stretching and ring breathing mode (~ 1620 cm^{-1}). Characteristic peaks for other carbon sources include stretching C-O deoxyribose (~ 1056 cm^{-1}), C-O stretching vibration (~ 1150 cm^{-1}), PO_2^- asymmetric (~ 1256 cm^{-1}), ring base (~ 1555 cm^{-1}) and lipids (~ 1740 cm^{-1}).

3.4 Mechanisms of Cd and Pb biosorption via spectral analysis

As fungal PTE-biosorption consists of two key stages as direct adsorption on fungal membrane and penetration through cell wall, they might be distinguished by analyzing the functional groups of cellular components or extracellular polymeric substance (EPS). Although PCA-LDA is applied to assess the 'fingerprint region' to characterize the relationships between the whole biospectra and fungal growth or biosorption efficiency, it is very challenging because the enormous spectral alterations across 48 different carbon sources (Figure 5A). We therefore attempted to identify discriminating alterations by introducing Pearson correlations to determine the relationships between microbial activities (e.g., biomass, Pb biosorption, Cd biosorption) and spectral variations based on cluster vector analysis. The results indicated that several discriminating alterations positively correlated with fungal biomass (Figure 5A), including 1340 cm^{-1} (collagen, $p<0.05$), 1136 cm^{-1} (collagen,

313 p<0.05) and 966 cm^{-1} (C-C DNA, p<0.05). These peaks could be viewed as
314 biomarkers for fungal growth (Figure 5B-5D). The significant peaks associated with
315 Cd biosorption included 1745 cm^{-1} (phospholipids, p<0.05), 1620 cm^{-1} (nucleic acid,
316 p<0.05), 1456 cm^{-1} (lipids and proteins, p<0.05), 1396 cm^{-1} (proteins, p<0.05) and
317 1057 cm^{-1} (stretching C-O deoxyribose, p<0.05), as illustrated in Figure 5E-5I.
318 However, there was no biomarker correlated with Pb biosorption, further confirming
319 the different biosorption mechanisms between Cd and Pb as suggested by the results
320 of biosorption isotherms.

321 ## 4. Discussion

322 ### *4.1 Biosorption capability of S. chinense QD10 on Cd and Pb*

323 Previous studies investigating microbes as biosorbents have demonstrated strong
324 capacities of microbial cells to absorb and remove PTEs, such as marine algae and
325 yeasts (Goyal et al., 2003; Özer and Özer, 2003; Volesky and Holan, 1995; Wang and
326 Chen, 2006). *Ascophyllum* and *Sargassum*, which can accumulate PTEs more than 30%
327 of dry weight biomass (Volesky and Holan, 1995). *Saccharomyces Cerevisiae* is a
328 species belonging to yeast, whose PTE biosorption capability ranges from 10 to 300
329 mg/g DCW for Pb and 10 to 100 mg/g DCW for Cd from the equilibrium biosorption
330 processes (Wang and Chen, 2006). PTE biosorption by fungi has also been
331 investigated, such as *Penicillium* sp. MRF-1 which has a strong biosorption capacity
332 of Cd (0.13-9.39 mg/g DCW) (Velmurugan et al., 2010) and *Exiguobacterium sp.*
333 with a maximum biosorption capacity of 15.6 mg/g DCW for Cd in Langmuir
334 isotherm (Park and Chon, 2016). In the present study, the biosorption capacity of *S.*
335 *chinense* QD10 was 0.77 mg/g DCW for Pb and 1.81 mg/g DCW for Cd, much lower
336 than a previous report on the same strain in rich medium (24.6 mg/g DCW for Cd and

31.2 mg/g DCW for Pb) (Jin et al., 2019). It might be attributing to the defined medium used in this study, which is nutrient deficient and cannot support the best fungal growth. Accordingly, fungal cells might not achieve optimal activities, resultsing in limited active binding sites on fungal cell membrane and lower Cd/Pb biosorption capacity by *S. chinense* QD10. However, defined medium fits better with the real scenarios in natural habitats, where microbes survive under nutrient depletion conditions (Jin et al., 2017a; Jin et al., 2018a). Our result provides a high-throughput and more comprehensive database to evaluate the PTE-biosorption performance of *S. chinense* QD10 regarding phytoremediation practices.

4.2 Biospectral fingerprints of S. chinense QD10

Biospectroscopy has a long history of studying biological cells. IR spectroscopy can be traced back to 1950s (Jin et al., 2017b) and has been extensively applied as a sensitive and rapid screening tool for characterizing microbes (Jin et al., 2017b; Picorel et al., 1991). Over the past 20 years, IR spectroscopy is successfully developed for examining biological molecules at cell or tissue level, including bacteria, yeast and mammalian cells (Baker et al., 2014; Martin et al., 2010; Movasaghi et al., 2008). However, only limited works focus on fungi, and there is lack of well-established database for fungal spectral biomarkers. In the present study, our results illustrated similar biospectra with several key biomarkers of fungi comparing to those of bacterial cells based on past literatures, including lipid (~ 1750 cm^{-1}), Amide I (~ 1650 cm^{-1}), Amide II (~ 1550 cm^{-1}), carbohydrate (~ 1155 cm^{-1}) and symmetric phosphate stretching vibrations (~ 1080 cm^{-1}) (Baker et al., 2014; Maquelin et al., 2003; Martin et al., 2010). It might be attributed to the similar cell wall components, such as lipids, proteins and carbohydrate, even though fungi are protected by a true cell wall (Sağ, 2001).

4.3 Spectral biomarkers for S. chinense QD10 growth across carbon source groups

Although the GI of *S. chinense* QD10 cultivated with different carbon source groups showed no significant difference, the cluster vector analysis raises more biochemical information by locating the discriminating biomarkers across carbon source categories. These biomarkers reveal the metabolic features of *S. chinense* QD10 responsive to carbon sources. Cultivated with carbohydrate, for instance, biospectra of *S. chinense* QD10 have specific biomarkers including PO_2^- asymmetric (~ 1265 cm^{-1}), RNA (~ 1117 cm^{-1}), CH in-plane bend (~ 1510 cm^{-1}), Amide I (~ 1659 cm^{-1}) and C=O, lipids (~ 1740 cm^{-1}), indicating the occurrence of complex carbohydrate metabolic processes during fungal growth (Figure 4). These biomarkers are significantly different from those linked with bacterial growth except for Amide I (~ 1659 cm^{-1}) (Jin et al., 2018a; Jin et al., 2018b), suggesting distinct metabolite profiles between fungal and bacterial growth. Carbohydrates are reported to associate with fungal metabolism, not only providing energy for the synthesis of trehalose, polyols, glycogen, fatty acids and other cellular components, but also supplying carbon skeleton for other metabolic processes, such as hyphal growth and amino acid biosynthesis (Bago et al., 2003; Deveau et al., 2008; Rasmussen et al., 2008). As the fungal metabolisms vary across intra- and inter-groups of different carbon sources throughout the growth period, there is no clear relationship between growth and carbon source categories.

We further applied Pearson correlation analysis based on cluster vector analysis to link the spectral variations with fungal biomass and identify some key biomarkers for fungal growth. The IR bands significantly correlated with GI include 1340 cm^{-1} (collagen), 1136 cm^{-1} (collagen) and 966 cm^{-1} (C-C DNA, Figure 5B-5D), implying

strong associations of these cellular components with fungal growth. Among them, the DNA-spectral biomarker represents DNA replication through cell reproduction process (Jin et al., 2018a; Jin et al., 2018b). Additionally, the collagen-associated spectral alterations are very likely linked to the formation of fungal fimbriae, which consist of collagen and are abundant on extracochlear surfaces (Celerin et al., 1996). Our results suggest that these spectral biomarkers can be used as fungal growth indicators in future studies.

4.4 Derived biospectral biomarkers explaining different mechanisms of Cd and Pb biosorption

Cultivated with different carbon sources, Cd and Pb biosorption by *S. chinense* QD10 followed the Langmuir and Freundlich isotherm, respectively. It implied distinct mechanisms behind Pb and Cd biosorption, consistent with our previous report (Jin et al., 2019). As the Langmuir isotherm represents the monolayer adsorption mechanism and the Freundlich isotherm describes both monolayer and multilayer adsorptions by considering the heterogeneous surfaces possessing different sorption energy sites, spectrochemical analysis might provide deeper insights *via* diagnosing spectral alterations associated with PTE biosorption process.

The results of spectral analysis indicate that phosphor-lipids and proteins (1745 cm^{-1}, 1456 cm^{-1}, 1396 cm^{-1}) are strongly correlated with Cd biosorption (Figure 5E-5I). It suggests that the cell wall components of *S. chinense* QD10 are the primary interactive targets for Cd biosorption, such as polysaccharides, proteins and lipids which offer abundant metal-binding functional groups, *e.g.*, carboxylate hydroxyl, sulphate, phosphate and amino groups (Veglio and Beolchini, 1997). It is consistent with the fact that Cd biosorption isotherm follows the Langmuir isotherm and is more

likely driven by the cell surface sorption that both proteins and carbohydrate fractions are involved in the binding of Cd ions (Jin et al., 2019). In contrast, no spectral biomarker is observed to significantly associate with Pb biosorption. This result is also evidenced by the Freundlich isotherm of Pb biosorption describing both monolayer and multilayer adsorptions by considering the heterogeneous surfaces. Thus, it suggests that extracellular precipitation explains the majority of Pb biosorption and EPS possess a substantial quantity of anion functional groups adsorbing Pb^{2+} ions (Wang and Chen, 2006).

This discrimination may be derived from the two stages of PTE biosorption mechanisms by fungi: direct adsorption on fungal membrane and penetration through cell wall (Leonard et al., 2004). These two stages can occur independently, possibly resulting in disticnt biosorption behaviour across biosorbents (microbial species) or PTEs. For instance, exopolysaccharides (EPS) represent an interesting affinity for Pb, which is a metabolism-independent process driven by interactions between the cations and negative charges of acidic functional groups of EPS (Pérez et al., 2008). As EPS are a mixture of biomaterials, such as EPS, glucoprotein, lipopolysaccharide and soluble peptide (Jin et al., 2019), it is very challenging to distinguish and extract specfic spectral biomarkers associated with extracellular components responsible for PTE biosorption. Our results hint that discriminating peaks derived from IR spectra could satisfactorily uncover the behaviour and mechanisms of PTE biosorption by interrogating the distinct functional groups or cellular components (Martin et al., 2010).

5. Conclusion and remarks

Fungi-assisted phytoremediation is an environmentally-safe approach to remove PTEs

from contaminated soils, and PTE biosorption by fungi is a critical step in phytoremediation. This study introduced ATR-FTIR spectroscopy coupled with Biolog PM plate as a non-destructive and high-throughput approach to investigate the performance and mechanisms of Cd and Pb biosorption by a fungal strain *S. chinense* QD10 cultivated with difference carbon sources. For the first time, we found several spectral biomarkers associated with the growth (1340 cm^{-1}, 1136 cm^{-1}, 966 cm^{-1}) and Cd biosorption (1745 cm^{-1}, 1620 cm^{-1}, 1456 cm^{-1}, 1396 cm^{-1}, 1057 cm^{-1}) of *S. chinense* QD10. Cd biosorption primarily followed the monolayer Langmuir isotherm and was mainly driven by the cell surface sorption, unravelled by the spectral alterations affiliated with proteins and carbohydrates (1745 cm-1, 1456 cm-1, 1396 cm^{-1}). For Pb biosorption, EPS possibely possessed a substantial quantity of anion functional groups adsorbing Pb^{2+} ions as extracellular precipitation, thus following multilayer Freundlich isotherm and representing no significant spectral biomarkers. Our results suggested biospectroscopy as a powerful tool in investigating the interactions between fungal cells and PTEs, distinguishing both functional groups and mechanisms associated with PTE biosorption process. This study lends new sights into fungal PTE biosorption and offers database of their behaviour across various carbon sources, revealing the tip of the iceberg regarding the interactions between microbes and PTEs in real-world scenario from spectroscopic perspective, which implies great potential for enhancing phytoremediation.

6. Declaration of Competing Interest

The authors declare that they have no known competing financial interests or personal relationships that could have appeared to influence the work reported in this paper.

7. Acknowledgements

This study was supported by the National Key Research and Development Program of China (2018YFC1800701), Natural Science Foundation of China (No. 41977346), China Postdoctoral Science Foundation (2019M650707), Natural Science Foundation of Heilongjiang Province (No. C201240) and Science and Technology Research Project of the Department of Education, Heilongjiang Province (No. 12531754). DZ also acknowledges the support of Chinese Government's Thousand Talents Plan for Young Professionals.

8. Reference

Ali, H., Khan, E., Sajad, M.A., 2013. Phytoremediation of heavy metals-Concepts and applications. Chemosphere 91, 869-881.

Bago, B., Pfeffer, P.E., Abubaker, J., Jun, J., Allen, J.W., Brouillette, J., Douds, D.D., Lammers, P.J., Shachar-Hill, Y., 2003. Carbon export from arbuscular mycorrhizal roots involves the translocation of carbohydrate as well as lipid. Plant Physiol 131, 1496-1507.

Baker, M.J., Trevisan, J., Bassan, P., Bhargava, R., Butler, H.J., Dorling, K.M., Fielden, P.R., Fogarty, S.W., Fullwood, N.J., Heys, K.A., Hughes, C., Lasch, P., Martin-Hirsch, P.L., Obinaju, B., Sockalingum, G.D., Sule-Suso, J., Strong, R.J., Walsh, M.J., Wood, B.R., Gardner, P., Martin, F.L., 2014. Using Fourier transform IR spectroscopy to analyze biological materials. Nat Protoc 9, 1771-1791.

Bolan, N., Kunhikrishnan, A., Thangarajan, R., Kumpiene, J., Park, J., Makino, T., Kirkham, M.B., Scheckel, K., 2014. Remediation of heavy metal(loid)s contaminated soils - To mobilize or to immobilize? J Hazard Mater 266, 141-166.

Butler, H.J., McAinsh, M.R., Adams, S., Martin, F.L., 2015. Application of vibrational spectroscopy techniques to non-destructively monitor plant health and development. Anal Methods 7, 4059-4070.

Celerin, M., Ray, J.M., Schisler, N.J., Day, A.W., Stetler-Stevenson, W.G., Laudenbach, D., 1996. Fungal fimbriae are composed of collagen. Embo J. 15, 4445.

Deng, S., Ke, T., Li, L., Cai, S., Zhou, Y., Liu, Y., Guo, L., Chen, L., Zhang, D., 2018a. Impacts of environmental factors on the whole microbial communities in the rhizosphere of a metal-tolerant plant: *Elsholtzia haichowensis* Sun. Environ. Pollut. 237, 1088-1097.

Deng, S.Q., Ke, T., Wu, Y.F., Zhang, C., Hu, Z.Q., Yin, H.M., Guo, L.M., Chen, L.Z., Zhang, D.Y., 2018b. Heavy Metal Exposure Alters the Uptake Behavior of 16 Priority Polycyclic Aromatic Hydrocarbons (PAHs) by Pak Choi (*Brassica chinensis* L.). Environ Sci Technol 52, 13457-13468.

Deveau, A., Kohler, A., Frey□Klett, P., Martin, F., 2008. The major pathways of carbohydrate metabolism in the ectomycorrhizal basidiomycete Laccaria bicolor S238N. New Phytol 180, 379-390.

Dong, X.Q., Li, C.L., Li, J., Wang, J.X., Liu, S.T., Ye, B., 2010. A novel approach for soil contamination assessment from heavy metal pollution: A linkage between discharge and adsorption. J Hazard Mater 175, 1022-1030.

Geelhoed, J.S., Meeussen, J.C.L., Roe, M.J., Hillier, S., Thomas, R.P., Farmer, J.G., Paterson, E., 2003. Chromium remediation or release? Effect of iron(II) sulfate addition on chromium(VI) leaching from columns of chromite ore processing residue. Environ Sci Technol 37, 3206-3213.

Gheju, M., Balcu, I., Mosoarca, G., 2016. Removal of Cr(VI) from aqueous solutions by adsorption on MnO_2. J Hazard Mater 310, 270-277.

Gordon, S., Jones, R., McClelland, J., Wicklow, D., Greene, R., 1999. Transient infrared spectroscopy for detection of toxigenic fungi in corn: potential for on-line evaluation. J Agr Food Chem 47, 5267-5272.

Goyal, N., Jain, S., Banerjee, U., 2003. Comparative studies on the microbial adsorption of heavy metals. Adv Environ Res 7, 311-319.

Hamdy, A., 2000. Biosorption of heavy metals by marine algae. Curr Microbiol 41, 232-238.

He, J., Chen, J.P., 2014. A comprehensive review on biosorption of heavy metals by algal biomass: materials, performances, chemistry, and modeling simulation tools. Bioresour Technol 160, 67-78.

Heys, K.A., Riding, M.J., Strong, R.J., Shore, R.F., Pereira, M.G., Jones, K.C., Semple, K.T., Martin, F.L., 2014. Mid-infrared spectroscopic assessment of nanotoxicity in gram-negative vs. gram-positive bacteria. Analyst 139, 896-905.

Huang, Y., Wang, L., Wang, W., Li, T., He, Z., Yang, X., 2019. Current status of agricultural soil pollution by heavy metals in China: A meta-analysis. Sci Total Environ 651, 3034-3042.

Järup, L., 2003. Hazards of heavy metal contamination. Brit Med Bull 68, 167-182.

Jiang, B., Adebayo, A., Jia, J., Xing, Y., Deng, S.Q., Guo, L.M., Liang, Y.T., Zhang, D.Y., 2019. Impacts of heavy metals and soil properties at a Nigerian e-waste site on soil microbial community. J Hazard Mater 362, 187-195.

Jiang, B., Xing, Y., Zhang, B.G., Cai, R.Q., Zhang, D.Y., Sun, G.D., 2018. Effective phytoremediation of low-level heavy metals by native macrophytes in a vanadium mining area, China. Environ Sci Pollut R 25, 31272-31282.

Jin, N., Morais, C.L.M., Martin, F.L., Zhang, D., 2020. Spectrochemical identification of kanamycin resistance genes in artificial microbial communities using Clover-assay. J Pharmaceut Biomed 181, 113108.

Jin, N., Paraskevaidi, M., Semple, K.T., Martin, F.L., Zhang, D.Y., 2017a. Infrared Spectroscopy Coupled with a Dispersion Model for Quantifying the Real-Time Dynamics of Kanamycin Resistance in Artificial Microbiota. Anal Chem 89, 9814-9821.

Jin, N.F., Semple, K.T., Jiang, L.F., Luo, C.L., Martin, F.L., Zhang, D.Y., 2018a. Spectrochemical determination of unique bacterial responses following long-term low-level exposure to antimicrobials. Anal Methods 10, 1602-1611.

Jin, N.F., Semple, K.T., Jiang, L.F., Luo, C.L., Zhang, D.Y., Martin, F.L., 2018b. Spectrochemical analyses of growth phase-related bacterial responses to low (environmentally-relevant) concentrations of tetracycline and nanoparticulate silver. Analyst 143, 768-776.

Jin, N.F., Zhang, D.Y., Martin, F.L., 2017b. Fingerprinting microbiomes towards screening for microbial antibiotic resistance. Integrative Biology 9, 406-417.

Jin, Z., Deng, S., Wen, Y., Jin, Y., Pan, L., Zhang, Y., Black, T., Jones, K.C., Zhang, H., Zhang, D., 2019. Application of *Simplicillium chinense* for Cd and Pb biosorption and enhancing heavy metal phytoremediation of soils. Sci Total Environ 697, 134148.

Khan, A.A., Muthukrishnan, M., Guha, B.K., 2010. Sorption and transport modeling of hexavalent chromium on soil media. J Hazard Mater 174, 444-454.

Khan, A.G., 2005. Role of soil microbes in the rhizospheres of plants growing on trace metal contaminated soils in phytoremediation. J Trace Elem Med Bio 18, 355-364.

Kos, G., Lohninger, H., Krska, R., 2002. Fourier transform mid-infrared spectroscopy with attenuated total reflection (FT-IR/ATR) as a tool for the detection of Fusarium fungi on maize. Vib Spectrosc 29, 115-119.

Leonard, S.S., Harris, G.K., Shi, X.L., 2004. Metal-induced oxidative stress and signal transduction. Free Radical Bio Med 37, 1921-1942.

Li, H.B., Martin, F.L., Zhang, D.Y., 2017. Quantification of Chemotaxis-Related Alkane Accumulation in *Acinetobacter baylyi* Using Raman Microspectroscopy. Anal. Chem. 89, 3909-3918.

Liu, M., Qiao, G., Jiang, J., Han, X., Sang, J., Zhuo, R., 2014. Identification and expression analysis of salt-responsive genes using a comparative microarray approach in Salix matsudana. Mol Biol Rep 41, 6555-6568.

Liu, M.Y., He, X.L., Feng, T.Y., Zhuo, R.Y., Qiu, W.M., Han, X.J., Qao, G.R., Zhang, D.Y., 2019. cDNA Library for Mining Functional Genes in Sedum alfredii Hance Related to Cadmium Tolerance and Characterization of the Roles of a Novel SaCTP2 Gene in Enhancing Cadmium Hyperaccumulation. Environ Sci Technol 53, 10926-10940.

Liu, X.M., Song, Q.J., Tang, Y., Li, W.L., Xu, J.M., Wu, J.J., Wang, F., Brookes, P.C., 2013. Human health risk assessment of heavy metals in soil-vegetable system: A multi-medium analysis. Sci Total Environ 463, 530-540.

Maquelin, K., Kirschner, C., Choo-Smith, L.-P., Ngo-Thi, N., Van Vreeswijk, T., Stämmler, M., Endtz, H., Bruining, H., Naumann, D., Puppels, G., 2003. Prospective study of the performance of vibrational spectroscopies for rapid identification of bacterial and fungal pathogens recovered from blood cultures. J Clin Microbiol 41, 324-329.

Martin, F.L., Kelly, J.G., Llabjani, V., Martin-Hirsch, P.L., Patel, I.I., Trevisan, J., Fullwood, N.J., Walsh, M.J., 2010. Distinguishing cell types or populations based on the computational analysis of their infrared spectra. Nat. Protoc. 5, 1748-1760.

Movasaghi, Z., Rehman, S., ur Rehman, D.I., 2008. Fourier Transform Infrared (FTIR) Spectroscopy of Biological Tissues. Appl Spectrosc Rev 43, 134-179.

Naumann, A., Navarro-González, M., Peddireddi, S., Kües, U., Polle, A., 2005. Fourier transform infrared microscopy and imaging: Detection of fungi in wood. Fungal Genet Biol 42, 829-835.

Ou, J., Li, H., Yan, Z., Zhou, Y., Bai, L., Zhang, C., Wang, X., Chen, G., 2018. In situ immobilisation of toxic metals in soil using Maifan stone and illite/smectite clay. Sci Rep 8, 1-9.

Özer, A., Özer, D., 2003. Comparative study of the biosorption of Pb (II), Ni (II) and Cr (VI) ions onto S. cerevisiae: determination of biosorption heats. J Hazard Mater 100, 219-229.

Pérez, J.A.M., García-Ribera, R., Quesada, T., Aguilera, M., Ramos-Cormenzana, A., Monteoliva-Sánchez, M., 2008. Biosorption of heavy metals by the exopolysaccharide produced by *Paenibacillus jamilae*. World J Microbiol Biotechnol 24, 2699.

Park, J.H., Chon, H.-T., 2016. Characterization of cadmium biosorption by Exiguobacterium sp. isolated from farmland soil near Cu-Pb-Zn mine. Environ Sci

Pollut R 23, 11814-11822.
Patterson, R.R., Fendorf, S., Fendorf, M., 1997. Reduction of hexavalent chromium by amorphous iron sulfide. Environ Sci Technol 31, 2039-2044.
Picorel, R., Holt, R.E., Heald, R., Cotton, T.M., Seibert, M., 1991. Stability of Isolated Bacterial and Photosystem-Ii Reaction Center Complexes on Ag Electrode Surfaces - a Surface-Enhanced Resonance Raman-Study. J Am Chem Soc 113, 2839-2843.
Rasmussen, S., Parsons, A.J., Fraser, K., Xue, H., Newman, J.A., 2008. Metabolic profiles of Lolium perenne are differentially affected by nitrogen supply, carbohydrate content, and fungal endophyte infection. Plant Physiol 146, 1440-1453.
Rui, D., Wu, Z., Ji, M., Liu, J., Wang, S., Ito, Y., 2019. Remediation of Cd- and Pb-contaminated clay soils through combined freeze-thaw and soil washing. J Hazard Mater 369, 87-95.
Sağ, Y., 2001. Biosorption of heavy metals by fungal biomass and modeling of fungal biosorption: a review. Sep Purif Methods 30, 1-48.
Sarkar, B., Xi, Y., Megharaj, M., Krishnamurti, G.S.R., Rajarathnam, D., Naidu, R., 2010. Remediation of hexavalent chromium through adsorption by bentonite based Arquad®2HT-75 organoclays. J Hazard Mater 183, 87-97.
Say, R., Denizli, A., Arıca, M.Y., 2001. Biosorption of cadmium (II), lead (II) and copper (II) with the filamentous fungus Phanerochaete chrysosporium. Bioresour Technol 76, 67-70.
Sha, H., Wu, Y., Fan, Y., 2018. Utilization of industrial waste as a novel adsorbent: Mono/competitive adsorption of chromium(VI) and nickel(II) using diatomite waste modified by EDTA. Appl Organomet Chem 32, e3977.
Shaheen, S.M., Wang, J.X., Swertz, A.C., Feng, X.B., Bolan, N., Rinklebe, J., 2019. Enhancing phytoextraction of potentially toxic elements in a polluted floodplain soil using sulfur-impregnated organoclay. Environ Pollut 248, 1059-1066.
Singh, R., Dong, H., Zeng, Q., Zhang, L., Rengasamy, K., 2017. Hexavalent chromium removal by chitosan modified-bioreduced nontronite. Geochim Cosmochim Ac 210, 25-41.
Tantawy, M.A., El-Roudi, A.M., Salem, A.A., 2012. Immobilization of Cr(VI) in bagasse ash blended cement pastes. Construction and Building Materials 30, 218-223.
Trevisan, J., Angelov, P.P., Scott, A.D., Carmichael, P.L., Martin, F.L., 2013. IRootLab: a free and open-source MATLAB toolbox for vibrational biospectroscopy data analysis. Bioinformatics 29, 1095-1097.
Veglio, F., Beolchini, F., 1997. Removal of metals by biosorption: a review. Hydrometallurgy 44, 301-316.
Velmurugan, N., Hwang, G., Sathishkumar, M., Choi, T.K., Lee, K.-J., Oh, B.-T., Lee, Y.-S., 2010. Isolation, identification, Pb (II) biosorption isotherms and kinetics of a lead adsorbing Penicillium sp. MRF-1 from South Korean mine soil. J Environ Sci-China 22, 1049-1056.
Volesky, B., Holan, Z., 1995. Biosorption of heavy metals. Biotechnol Progr 11, 235-250.
Wang, J., Chen, C., 2006. Biosorption of heavy metals by Saccharomyces cerevisiae: a review. Biotechnol Adv 24, 427-451.

Wang, J., Chen, C., 2014. Chitosan-based biosorbents: modification and application for biosorption of heavy metals and radionuclides. Bioresour Technol 160, 129-141.

Wang, S., Vipulanandan, C., 2001. Solidification/stabilization of Fe(II)-treated Cr(VI)-contaminated soil. Environ Eng Sci 18, 301-308.

Wiszniewska, A., Hanus-Fajerska, E., Muszynska, E., Ciarkowska, K., 2016. Natural Organic Amendments for Improved Phytoremediation of Polluted Soils: A Review of Recent Progress. Pedosphere 26, 1-12.

Yan, G., Viraraghavan, T., 2003. Heavy-metal removal from aqueous solution by fungus *Mucor rouxii*. Water Res 37, 4486-4496.

Yin, H., Niu, J., Ren, Y., Cong, J., Zhang, X., Fan, F., Xiao, Y., Zhang, X., Deng, J., Xie, M., He, Z., Zhou, J., Liang, Y., Liu, X., 2015. An integrated insight into the response of sedimentary microbial communities to heavy metal contamination. Sci Rep 5, 14266.

Yuan, W.Y., Xu, W.T., Wu, Z.B., Zhang, Z.W., Wang, L.C., Bai, J.F., Wang, X.Y., Zhang, Q.W., Zhu, X.F., Zhang, C.L., Wang, J.W., 2018. Mechanochemical treatment of Cr(VI) contaminated soil using a sodium sulfide coupled solidification/stabilization process. Chemosphere 212, 540-547.

Zhang, D., Fakhrullin, R.F., Özmen, M., Hui, W., Jian, W., Paunov, V.N., Li, G., Huang, W.E., 2011. Functionalization of whole□cell bacterial reporters with magnetic nanoparticles. Microb Biotechnol 4, 89-97.

9. Figure Captions

Figure 1. Growth profiles of *S. chinense* QD10 with 48 different carbon sources. (A) Growth curves during a 144-hour cultivation period. (B) Growth indices (GI) of *S. chinense* QD10 in comparison with the negative control (A1, no carbon source).

Figure 2. Cd and Pb adsorption isotherms by *S. chinense* QD10 cultivated with 48 different carbon sources. (A) Langmuir isotherm model representing the monolayer adsorption mechanism. (B) Freundlich isotherm model representing both monolayer and multilayer adsorptions by considering the heterogeneous surfaces possessing different sorption energy sites. Initial concentration of Cd and Pb was 100 mg/L and the adsorption time was 2 hours.

Figure 3. (A) Mean spectra of all pre-processed data of *S. chinense* QD10 cultivated with 48 different carbon sources based on rubberband baseline correction and Amide I (1650 cm^{-1}) normalization. (B) PCA-LDA categorizations of *S. chinense* QD10 cultivated with five groups of carbon sources, including nucleic acid, carbohydrate, carboxylic acid, amino acid and others. Twenty infrared spectra were randomly obtained per treatment. Different small letters indicate significant difference (Duncan's test, $p<0.05$) among treatments.

Figure 4. Cluster vector analysis of *S. chinense* QD10 cultivated with five groups of carbon sources. The unique spectral biomarkers for each carbon source group are labelled. Twenty infrared spectra were randomly obtained per treatment.

Figure 5. (A) Cluster vector of *S. chinense* QD10 cultivated with 48 different carbon sources. Colour bars illustrate IR bands possessing significant correlations ($p<0.05$) with growth index (GI, green), Pb biosorption efficiency (blue) and Cd biosorption efficiency (red). IR bands significantly correlate with GI include: (B) 1340 cm^{-1}

688 (collagen), (C) 1136 cm^{-1} (collagen) and (D) 966 cm^{-1} (C-C DNA). IR bands
689 significantly correlate with Cd biosorption efficiency include: (E) 1745 cm^{-1}
690 (phospholipids), (F) 1620 cm^{-1} (nucleic acid), (G) 1456 cm^{-1} (lipids and proteins), (H)
691 1396 cm^{-1} (proteins) and (I) 1057 cm^{-1} (stretching C-O deoxyribose).

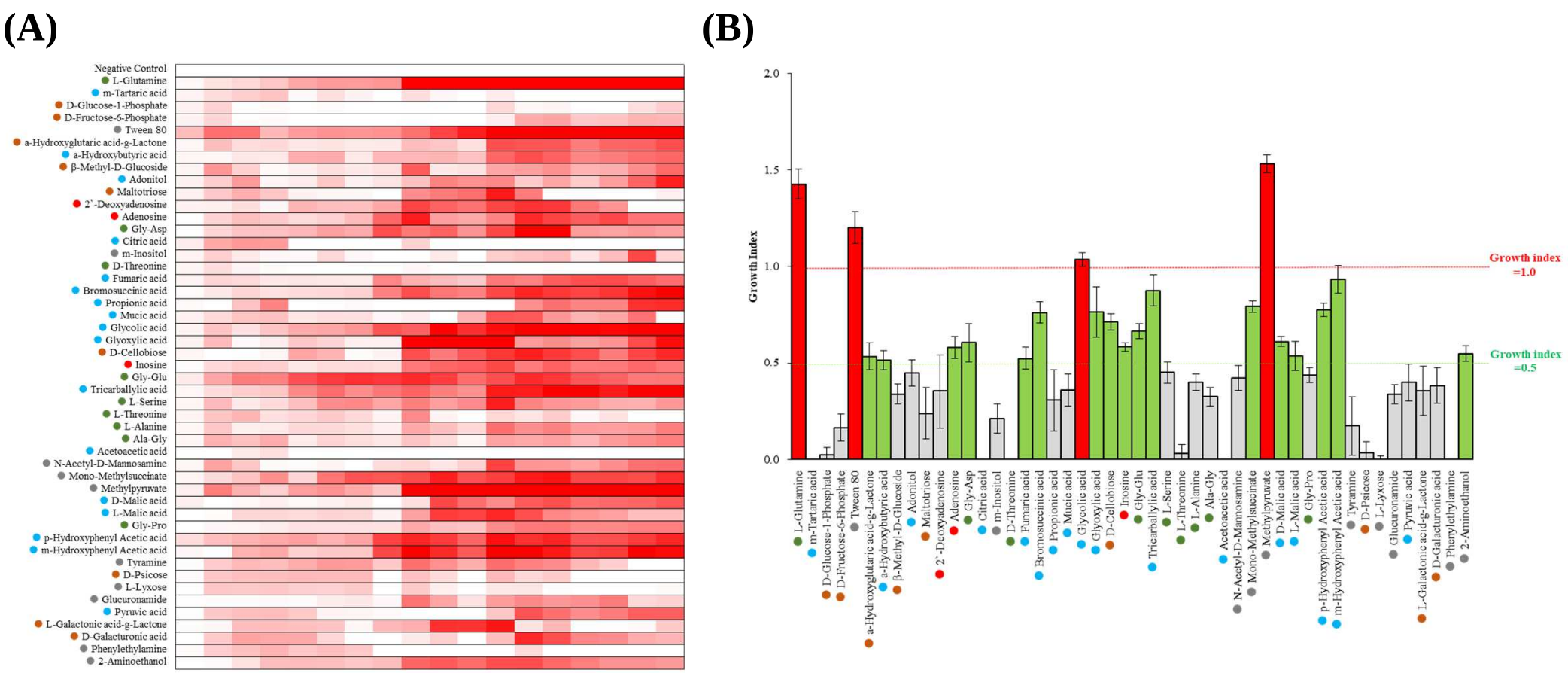
(A)
Negative Control
L-Glutamine
m-Tartaric acid
D-Glucose-1-Phosphate
D-Fructose-6-Phosphate
Tween 80
a-Hydroxyglutaric acid-g-Lactone
a-Hydroxybutyric acid
β-Methyl-D-Glucoside
Adonitol
Maltotriose
2`-Deoxyadenosine
Adenosine
Gly-Asp
Citric acid
m-Inositol
D-Threonine
Fumaric acid
Bromosuccinic acid
Propionic acid
Mucic acid
Glycolic acid
Glyoxylic acid
D-Cellobiose
Inosine
Gly-Glu
Tricarballylic acid
L-Serine
L-Threonine
L-Alanine
Ala-Gly
Acetoacetic acid
N-Acetyl-D-Mannosamine
Mono-Methylsuccinate
Methylpyruvate
D-Malic acid
L-Malic acid
Gly-Pro
p-Hydroxyphenyl Acetic acid
m-Hydroxyphenyl Acetic acid
Tyramine
D-Psicose
L-Lyxose
Glucuronamide
Pyruvic acid
L-Galactonic acid-g-Lactone
D-Galacturonic acid
Phenylethylamine
2-Aminoethanol
(B)
Growth Index
2.0
1.5
1.0
0.5
0.0
Growth index =1.0
Growth index =0.5
L-Glutamine
m-Tartaric acid
D-Glucose-1-Phosphate
D-Fructose-6-Phosphate
Tween 80
a-Hydroxyglutaric acid-g-Lactone
a-Hydroxybutyric acid
β-Methyl-D-Glucoside
Adonitol
Maltotriose
2`-Deoxyadenosine
Adenosine
Gly-Asp
Citric acid
m-Inositol
D-Threonine
Fumaric acid
Bromosuccinic acid
Propionic acid
Mucic acid
Glycolic acid
Glyoxylic acid
D-Cellobiose
Inosine
Gly-Glu
Tricarballylic acid
L-Serine
L-Threonine
L-Alanine
Ala-Gly
Acetoacetic acid
N-Acetyl-D-Mannosamine
Mono-Methylsuccinate
Methylpyruvate
D-Malic acid
L-Malic acid
Gly-Pro
p-Hydroxyphenyl Acetic acid
m-Hydroxyphenyl Acetic acid
Tyramine
D-Psicose
L-Lyxose
Glucuronamide
Pyruvic acid
L-Galactonic acid-g-Lactone
D-Galacturonic acid
Phenylethylamine
2-Aminoethanol

Figure 1

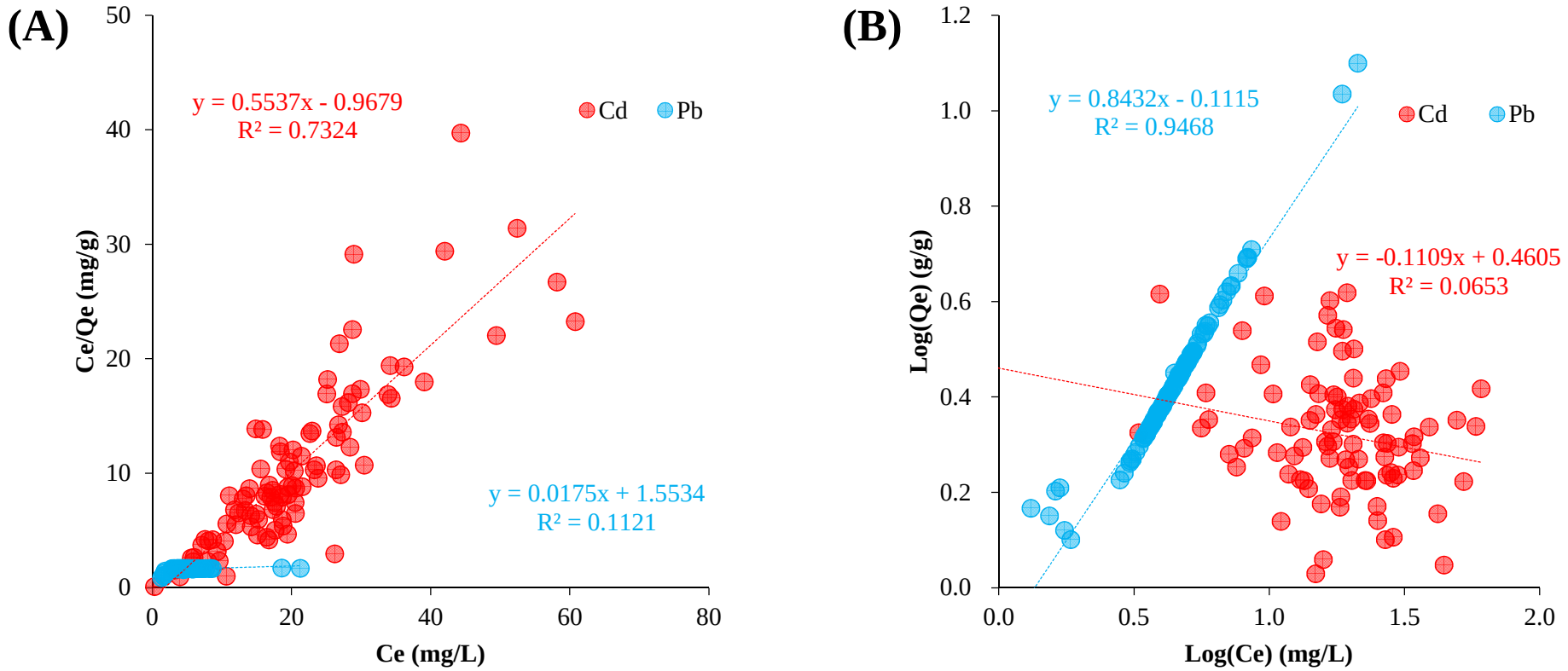
(A)
y = 0.5537x - 0.9679
R² = 0.7324
Cd
Pb
y = 0.0175x + 1.5534
R² = 0.1121
Ce/Qe (mg/g)
Ce (mg/L)
0
10
20
30
40
50
0
20
40
60
80
(B)
y = 0.8432x - 0.1115
R² = 0.9468
Cd
Pb
y = -0.1109x + 0.4605
R² = 0.0653
Log(Qe) (g/g)
Log(Ce) (mg/L)
0.0
0.2
0.4
0.6
0.8
1.0
1.2
0.0
0.5
1.0
1.5
2.0

Figure 2

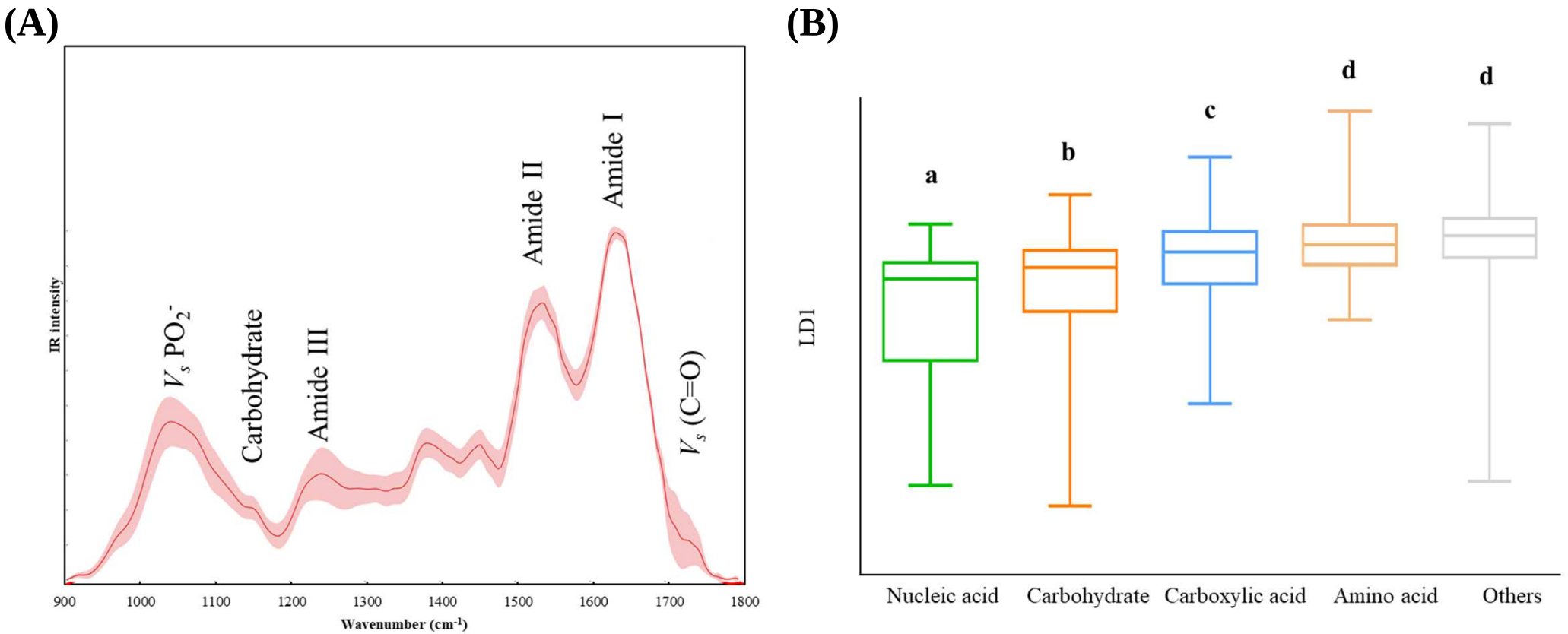
(A)
IR intensity
V_s PO_2^-
Carbohydrate
Amide III
Amide II
Amide I
V_s (C=O)
900
1000
1100
1200
1300
1400
1500
1600
1700
1800
Wavenumber (cm^{-1})
(B)
LD1
a
b
c
d
d
Nucleic acid
Carbohydrate
Carboxylic acid
Amino acid
Others

Figure 3

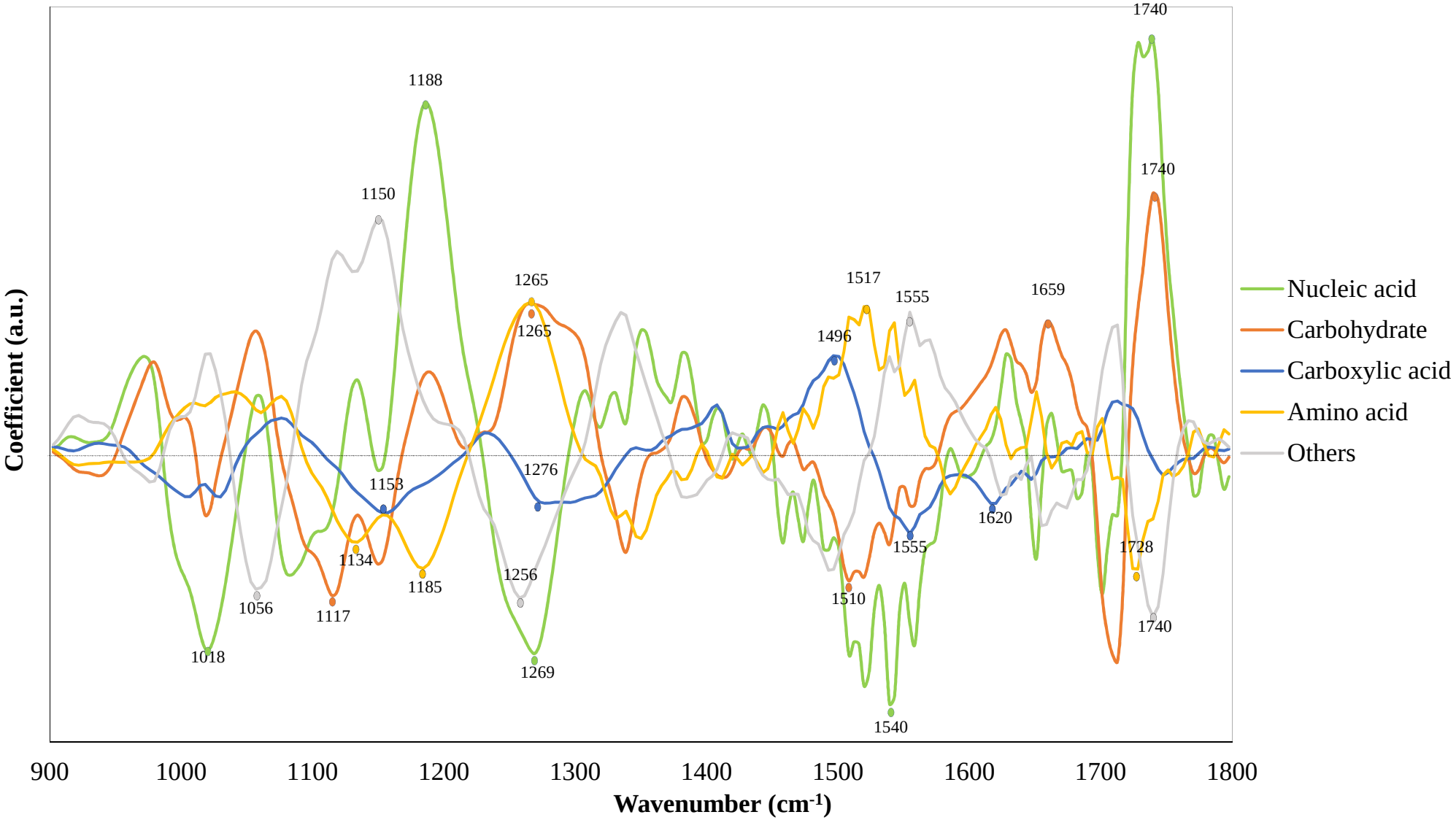
Coefficient (a.u.)
Wavenumber (cm-1)
900
1000
1100
1200
1300
1400
1500
1600
1700
1800
1740
1188
1150
1740
1265
1517
1555
1659
1265
1496
1276
1153
1620
1555
1728
1134
1256
1185
1510
1740
1056
1117
1018
1269
1540
Nucleic acid
Carbohydrate
Carboxylic acid
Amino acid
Others

Figure 4

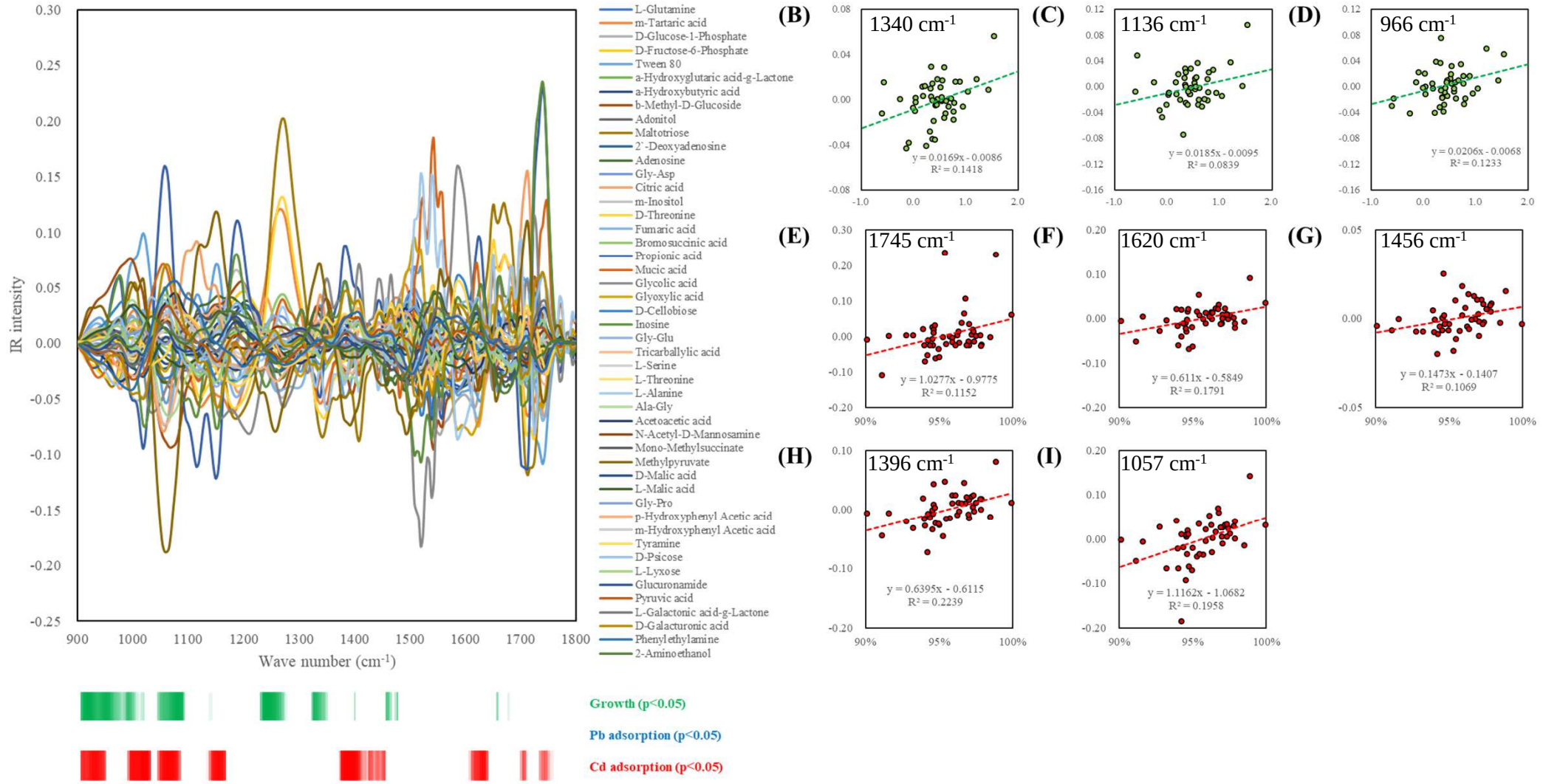
(A)
IR intensity
Wave number (cm-1)
L-Glutamine
m-Tartaric acid
D-Glucose-1-Phosphate
D-Fructose-6-Phosphate
Tween 80
a-Hydroxyglutaric acid-g-Lactone
a-Hydroxybutyric acid
b-Methyl-D-Glucoside
Adonitol
Maltotriose
2'-Deoxyadenosine
Adenosine
Gly-Asp
Citric acid
m-Inositol
D-Threonine
Fumaric acid
Bromosuccinic acid
Propionic acid
Mucic acid
Glycolic acid
Glyoxylic acid
D-Cellobiose
Inosine
Gly-Glu
Tricarballylic acid
L-Serine
L-Threonine
L-Alanine
Ala-Gly
Acetoacetic acid
N-Acetyl-D-Mannosamine
Mono-Methylsuccinate
Methylpyruvate
D-Malic acid
L-Malic acid
Gly-Pro
p-Hydroxyphenyl Acetic acid
m-Hydroxyphenyl Acetic acid
Tyramine
D-Psicose
L-Lyxose
Glucuronamide
Pyruvic acid
L-Galactonic acid-g-Lactone
D-Galacturonic acid
Phenylethylamine
2-Aminoethanol
Growth (p<0.05)
Pb adsorption (p<0.05)
Cd adsorption (p<0.05)
(B) 1340 cm-1 y = 0.0169x - 0.0086 R² = 0.1418
(C) 1136 cm-1 y = 0.0185x - 0.0095 R² = 0.0839
(D) 966 cm-1 y = 0.0206x - 0.0068 R² = 0.1233
(E) 1745 cm-1 y = 1.0277x - 0.9775 R² = 0.1152
(F) 1620 cm-1 y = 0.611x - 0.5849 R² = 0.1791
(G) 1456 cm-1 y = 0.1473x - 0.1407 R² = 0.1069
(H) 1396 cm-1 y = 0.6395x - 0.6115 R² = 0.2239
(I) 1057 cm-1 y = 1.1162x - 1.0682 R² = 0.1958

Figure 5

Highlights

1) Cd/Pb biosorption performance by *S. chinense* QD10 across 48 carbon sources

2) Langmuir model for Cd biosorption and Freundlich model for Pb biosorption

3) First ATR-FTIR spectroscopic study on metal biosorption mechanisms

4) Novel spectral biomarkers for fungal growth and Cd biosorption

Declaration of interests

☒ The authors declare that they have no known competing financial interests or personal relationships that could have appeared to influence the work reported in this paper.

☐The authors declare the following financial interests/personal relationships which may be considered as potential competing interests: